Hindawi
Mathematical Problems in Engineering
Volume 2021, Article ID 6640777, 8 pages
https://doi.org/10.1155/2021/6640777

Research Article

Calculation of Negative Frictional Resistance of Foundation Pile in Deep Fill Foundation

Ningyu Zhao,[1,2] **Hongjun Wu**,[2] **Yi Song**,[2] **and Shun Xiang**[2]

[1]*State Key Laboratory of Mountain Bridge and Tunnel Engineering, Chongqing Jiaotong University, Chongqing 400074, China*
[2]*School of Civil Engineering, Chongqing Jiaotong University, Chongqing 400074, China*

Correspondence should be addressed to Ningyu Zhao; zhny@cqjtu.edu.cn

Received 4 November 2020; Revised 30 December 2020; Accepted 30 January 2021; Published 27 February 2021

Academic Editor: Hussein Abulkasim

In deep fill foundations, the pile foundation might suffer from negative frictional resistance (NFR) due to the consolidation and settlement of the soil. The NFR will cause the pile to settle excessively and reduce its bearing capacity. However, there are not yet many accurate methods to calculate the NFR of foundation piles in deep fill foundations. To make up for the gap, this paper carries out shear tests on the pile-soil interface and discusses the mechanism of pile-side frictional resistance. Considering the distribution law of pile-side frictional resistance with depth, the authors proposed a piecewise calculation model for pile-side frictional resistance, which couples the hyperbolic model and effective stress method. Then, the energy balance equation of the pile when the NFR occurs was established in the light of the energy transfer of the pile-soil system during the settlement of the soil around the pile. Furthermore, the calculation formulas of the axial force and displacement of the pile at different depths were derived, considering the pile-soil displacement and the potential energy change of the pile-soil system. The proposed method was applied to calculate the NFR of the foundation pile in a construction site, and the calculated results were compared with the measured data. The results show that the axial force-depth curve of the pile obtained through theoretical calculation agrees well with the measured data. Hence, our method can accurately reveal the mechanical features of the pile foundation in deep fill foundations.

1. Introduction

In mountainous and hilly areas, the foundation of construction sites often features undulating bedrock surfaces and deep fills. If the superstructure has a large load, the deep foundation structure needs to meet a high settlement requirement. In this case, pile foundation is one of the few deep foundation structures that can be built directly on the said foundation.

Prior to the construction of the pile foundation, the filling site usually undergoes years of foundation treatments, such as self-weight consolidation and dynamic compaction. Although most of these deep fills have completed consolidation and settlement, negative frictional resistance (NFR) will be induced by the compressive deformation and incomplete consolidation of the foundation soil.

The relative displacement between the pile and the soil has a great impact on the distribution and magnitude of the pile-side frictional resistance, especially at the neutral point. The calculation of pile-soil displacement is very important for accurately predicting the influence of the pull-down load caused by NFR on the bearing capacity design of the pile foundation.

Many scholars have attempted to calculate the NFR of pile foundation. For instance, Zhang et al. [1] combined the effective stress method with Terzaghi's theory of one-dimensional (1D) consolidation to identify the NFR features of precast concrete (PCC) piles. Chen et al. [2] proved that the pile-side NFR can be simplified into a linear model by the effective stress method. Poulos et al. [3–5] proposed the elastic theory method based on Mindlin's solution and obtained the size and distribution of pile-side NFR using the differential equation of the pile body. Drawing on Kezdi's double-broken-line model, Zhao et al. [6] designed a load transfer model based on the effect of the pile-soil displacement and deduced the piecewise analytical solution of

the pile-side frictional resistance on each soil layer. Considering the effects of effective stress and pile-soil displacement on pile-side frictional resistance, He et al. [7] established a calculation model for the friction on the side of the rock-socketed pile by the load transfer method and iteratively computed the analytical solution of the axial force and the solution of power series for pile displacement. Chen et al. [8] summarized the results of soil structure interaction (SSI) tests, improved the hyperbolic model considering the change of initial shear stiffness and the shear features of the pile-soil system, and applied the improved model to disclose the change law of NFR and maximum axial force.

To sum up, the above studies mainly adopt four methods, namely, elastic theory method, effective stress method, load transfer method, and shear displacement method. Among them, the elastic theory method has a large error except for end-bearing piles, for the neglection of the effects of pile-soil displacement and inability to acquire accurate parameters. Despite its simple and easy-to-use formula, the effective stress method only applies to the situation with small pile-soil displacement because of the relatively large calculation result. The model of the load transfer method is too complex to be solved easily. The shear displacement method ignores the stress state of the foundation soil, the layering features, and the pile-top settlement.

These methods seldom consider the essence of negative skin friction, that is, the potential energy loss of soil around the pile and the process of energy transfer to the pile body. Studies have shown that the NFR hinges on the gravitational potential lost during the settlement of the surrounding soil and its shear strength [9]. Therefore, the NFR calculation should consider how the change in the potential energy of the pile-soil system affects the pile-side NFR.

To disclose the influence of energy conversion on the evolution of pile-side NFR, this paper analyzes the change law of the shear stress/normal stress-shear displacement ($\tau/\sigma_n - u$) curve through shear tests on the pile-soil interface. Then, a piecewise calculation model was constructed for pile-side frictional resistance in the light of the pile-soil displacement. Based on the reciprocal theorem, the control equations of the axial force and displacement of the pile were derived under different pile-soil displacements and solved by the iterative method. The proposed method was proved feasible and accurate by comparing the calculation results with the measured data.

2. Calculation Models

2.1. Calculation Model of Pile-Side Frictional Resistance. The relative displacement on the pile-soil interface is the root cause of pile-side frictional resistance. To calculate pile-side frictional resistance, the key lies in setting up a suitable pile-soil displacement model. Moreover, the shear features of the pile-soil interface inevitably change with the normal stress, before and during the shearing of that interface [10]. Therefore, the normal stress must be considered in the calculation model of pile-side frictional resistance.

To study the load transfer function of pile-side frictional resistance in deep fill, shear tests were carried out on the pile-soil interface in a deep fill site under different normal stresses ($\sigma_n = 100$, 200, and 400 kPa). The shear stress-shear displacement curves of the pile-soil interface were normalized into the $\tau/\sigma_n - u$ curves (Figure 1).

As shown in Figure 1, the shear stress reached the limit state at the pile-soil displacement of 6 mm. Before that, the $\tau/\sigma_n - u$ curves were hyperbolic. Therefore, the stress state before the full exertion of pile-side frictional resistance can be simulated well by the hyperbolic model reflecting the pile-soil displacement and the lateral pressure of the surrounding soil. After the shear displacement of the pile-soil system arrived at the limit state, the shear stress/normal stress (τ/σ_n) remained constant.

In deep fill foundations, the settlement of soil around the pile decreases with the depth, while the settlement of the pile-bottom is a certain value under the load of the pile, and the compression deformation of the pile decreases with the depth. The displacement of the soil above the neutral point is greater than that of the pile, and the pile body above the depth is subject to NFR. When the relative displacement of pile-soil is greater than the limit relative displacement, the NFR changes greatly. The relative displacement of pile-soil decreases with the depth, and the relative displacement at the neutral point is zero. The displacement of the pile below the neutral point is greater than that of the soil, and the pile is subject to positive friction resistance (PFR), and the pile-soil relative displacement increases gradually with the decrease of soil settlement.

According to the above shear features of the pile-soil interface and the distribution law of pile-side frictional resistance with depth, the calculation of pile-side frictional resistance can be illustrated by the sketch map in Figure 2.

As shown in Figure 2, the pile-side frictional resistance can be calculated in three segments:

(1) The first segment is the NFR growth segment, where pile-soil displacement is greater than ultimate relative displacement ($s - s_p > u_m$), and the NFR increases with the vertical effective stress of the soil; in this segment, the pile-side frictional resistance is calculated by effective stress method

(2) The second segment is the transition segment from NFR to positive frictional resistance (PFR), where pile-soil displacement is smaller than ultimate relative displacement ($|s - s_p| \le u_m$); in this segment, the pile-side frictional resistance is calculated by the hyperbolic formula, which considers the lateral pressure of the surrounding soil

(3) The third segment is where the pile-soil displacement exceeds the ultimate relative displacement ($s_p - s > u_m$); in this segment, the PFR equals the ultimate frictional resistance τ_m

Under the above conditions, the calculation model of pile-side frictional resistance can be established as follows:

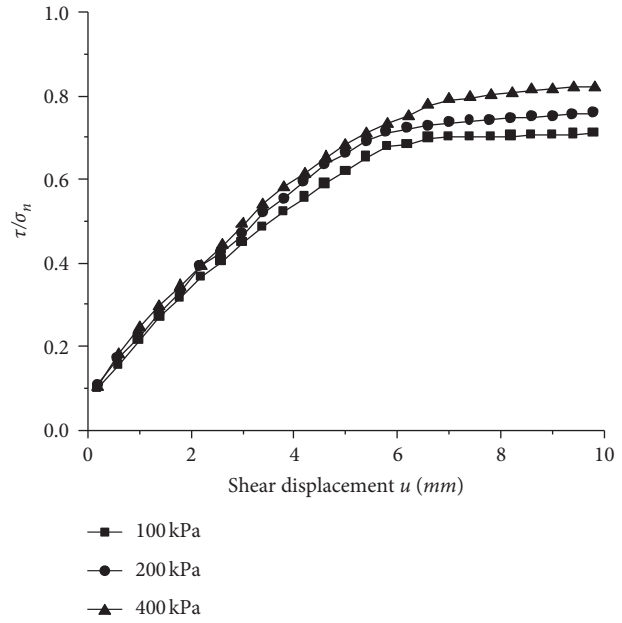

Figure 1: The $\tau/\sigma_n - u$curves.

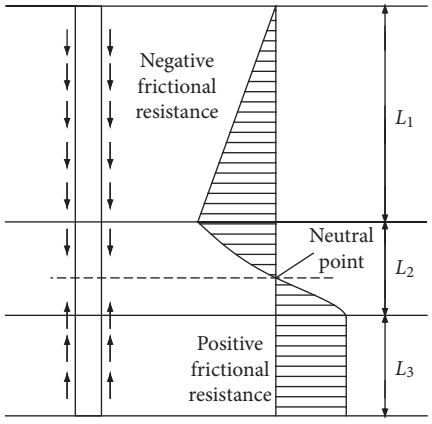

Figure 2: The calculation of pile-side frictional resistance.

$$\tau(z) = \begin{cases} \beta(q + \gamma' z), & s - s_p > u_m, \\ \dfrac{u\sigma_n}{A + Bu}, & |s - s_p| \le u_m, \\ \tau_m, & s_p - s > u_m, \end{cases} \quad (1)$$

where s_p and s are the settlements of the pile and the surrounding soil, respectively; β is the coefficient of frictional resistance; q is the overload acting on the ground;γ' is the weight of soil per unit volume; u_m is the ultimate relative displacement of the surrounding soil; $u$is the relative displacement;σ_n is the Earth pressure at rest; A and B are fitting parameters; τ_m is the ultimate frictional resistance.

The A and B values of the hyperbolic curve before the full exertion of the pile-side frictional resistance at the deep fill site were obtained by fitting the data of the $\tau/\sigma_n - u$ curves prior to the ultimate shear displacement with the hyperbolic formula in formula (1). The fitting results are presented in Figure 3.

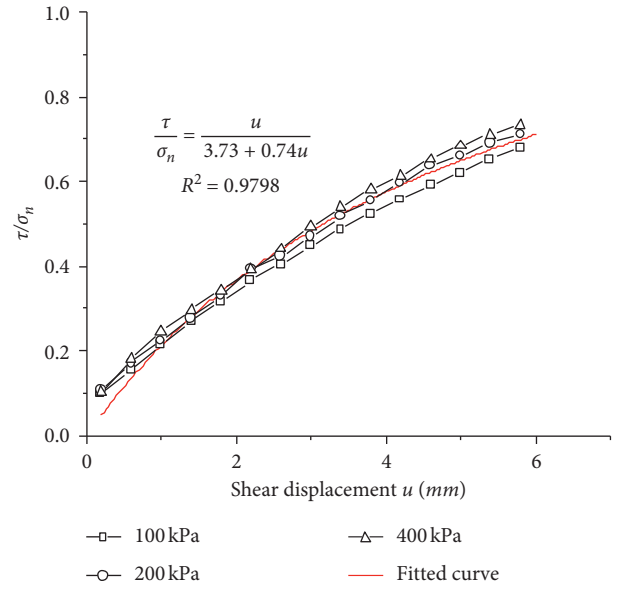

Figure 3: The fitted curve for pile-soil load transfer function.

From the $\tau/\sigma_n - u$ curves in Figure 3, it can be obtained that the fitting parameters $A = 3.73$, $B = 0.74$, and the coefficient of determination $R^2 = 0.9798$. Substituting A and B into formula (1), the transfer function of pile-side frictional resistance in the elastic state can be obtained.

2.2. Calculation of Pile-Bottom Resistance. Within the elastic range, the pile-bottom settlement basically has a linear relationship with pile-bottom resistance [11–14], and the pile-bottom settlement increases with pile-top settlement. Since the current code [15] forbids excessive pile-top settlement, it is assumed that the pile-bottom bearing layer does not have plastic deformation. Considering the pile-bottom as a rigid pressure block, it is realistic to calculate pile-bottom settlement by the Boussinesq equation [16]:

$$s_b = \frac{(1 - \mu_b)P_b}{4r_0 G_b}, \quad (2)$$

where r_0 is the radius of the pile; μ_b is Poisson's ratio of the soil at the pile-top; P_b is the pile-bottom resistance; and $G_b$is the shear modulus.

3. Building and Solving Energy Balance Equations

According to the NFR transfer law of piles in deep fill sites [17–20], and considering the engineering practicability of the mechanical model, the following assumptions were put forward before setting up the energy balance equations for the pile-soil system by the energy method:

(1) Under the pile-top load, the pile-side frictional resistance is exerted before the pile-top resistance

(2) The pile only suffers from elastic deformation rather than plastic deformation

(3) The pile elements are only affected by the vertical load.

3.1. Energy Balance Equations of the Pile-Soil System. The total potential energy of the pile-soil system in the foundation consists of the deformation energy of the pile, the potential energy increment caused by settlement, and the potential energy of the external forces [21]. The potential energy of the pile can be expressed as follows:

$$\Pi_p = \frac{1}{2}\int_0^L E_p A_p \left(\frac{\mathrm{d}\Delta}{\mathrm{d}z}\right)^2 dz - mg\left(s_b + \frac{\Delta}{2}\right), \tag{3}$$

where $L$is the pile length; $E_p$is the elastic modulus of the pile; $A_p$is the cross-sectional area of the pile; Δ is the deformation of the pile; $s_b$is pile-bottom displacement; m is the mass of the pile; and g is the acceleration of gravity.

The potential energy of the external force mainly encompasses the work of the pile-top load, the work of the pile-top resistance, and the work of the pile-side frictional resistance. Hence, the potential energy of the external forces can be expressed as follows:

$$\Pi_w = P_0 s_0 + \iint \tau(z)\left(s_b + \frac{\Delta}{2}\right)\mathrm{d}S - P_b s_b, \tag{4}$$

where P_0, P_b are pile-top load and pile-bottom load, respectively, and s_0 is pile-top displacement.

Based on the reciprocal theorem, the potential energy of the pile equals the total potential energy of the external forces acting on the pile. Combining formulas (3) and (4),

$$\begin{aligned}&\frac{1}{2}\int_0^L E_p A_p \left(\frac{d\Delta}{dz}\right)^2 \mathrm{d}z - mg\left(s_b + \frac{\Delta}{2}\right)\\ &\quad = P_0 s_0 + \iint \tau(z)\left(s_b + \frac{\Delta}{2}\right)\mathrm{d}S - P_b s_b.\end{aligned} \tag{5}$$

From the pile-top, the pile was discretized into n units (Figure 4). The nodes are denoted in turn as 0, 1, 2, . . ., $i-1$, i, $i+1$, . . ., n. The length of each element is $h = l/n$. The ith unit can be analyzed as follows:

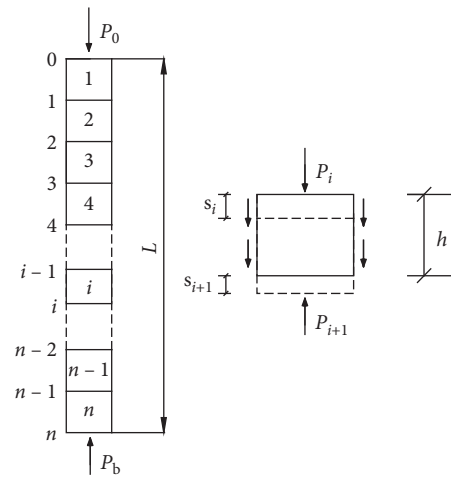

Figure 4: The discretization of the foundation pile.

$$\Delta_i = s_{pi} - s_{p(i+1)}, \tag{6}$$

$$\frac{\mathrm{d}\Delta_i}{\mathrm{d}z} = \frac{s_{pi} - s_{p(i+1)}}{h}, \tag{7}$$

where h is the length from the bottom to the top of the ith unit; Δ_i is the deformation of the ith unit; s_{pi} is the pile-top displacement of the ith unit; and $s_{p(i+1)}$is the pile-bottom displacement of the ith unit.

For the ith unit, substituting formulas (6) and (7) into formula (5):

$$\begin{aligned}P_i s_{pi} - P_{i+1} s_{p(i+1)} = \frac{1}{2}\int_{l_i}^{l_{i+1}} \cdot \Bigg\{ & E_p A_p \left(\frac{s_{pi} - s_{p(i+1)}}{h}\right)^2 - 2\pi r_0 \\ & \times \left(\tau_i s_{pi} + \tau_{i+1} s_{p(i+1)}\right)\Bigg\}\mathrm{d}z \\ & - \frac{mg}{2}\left(s_{pi} + s_{p(i+1)}\right).\end{aligned} \tag{8}$$

Integrating the right part of formula (8):

$$P_i s_{pi} - P_{i+1} s_{p(i+1)} = \frac{E_p A_p}{2h}\left(s_{pi} - s_{p(i+1)}\right)^2 - \pi r_0 h\left(\tau_i s_{pi} + \tau_{i+1} s_{p(i+1)}\right) - \frac{mg}{2}\left(s_{pi} + s_{p(i+1)}\right). \tag{9}$$

Expanding formula (9) and merging similar terms:

$$\begin{aligned}P_i s_{pi} - P_{i+1} s_{p(i+1)} = & \left\{\frac{E_p A_p}{2h}\left(s_{pi} - s_{p(i+1)}\right) - \pi r_0 h\tau_i - \frac{mg}{2}\right\} \\ & \cdot s_{pi} - \left\{\frac{E_p A_p}{2h}\left(s_{pi} - s_{p(i+1)}\right) + \pi r_0 h\tau_{i+1} + \frac{mg}{2}\right\} s_{p(i+1)}.\end{aligned} \tag{10}$$

Judging by the structure on both sides, formula (10) holds only if

$$P_i = \frac{E_p A_p}{2h}\left(s_{pi} - s_{p(i+1)}\right) - \pi r_0 h \tau_i - \frac{mg}{2}, \tag{11}$$

$$P_{i+1} = \frac{E_p A_p}{2h}\left(s_{pi} - s_{p(i+1)}\right) + \pi r_0 h \tau_{i+1} + \frac{mg}{2}. \tag{12}$$

The top pressure and bottom axial force in each unit can be solved by formulas (11) and (12).

The pile-bottom deformation of each unit can be obtained by transforming formula (11):

$$s_{p(i+1)} = s_{pi} - \frac{2h}{E_p A_p}\left(P_i + \pi r_0 h \tau_i + \frac{mg}{2}\right). \tag{13}$$

Substituting formula (1) into formulas (11) and (13), the axial force and displacement at each position of the pile can be obtained.

If $s - s_p > u_m$, then

$$P_i = \frac{E_p A_p}{2h}\left(s_{pi} - s_{p(i+1)}\right) - \pi r_0 h \beta\left(q + \gamma' z\right) - \frac{mg}{2}, \tag{14}$$

$$s_{p(i+1)} = s_{pi} - \frac{2h}{E_p A_p}\left(P_i + \pi r_0 h \beta\left(q + \gamma' z\right) + \frac{mg}{2}\right). \tag{15}$$

If $|s - s_p| \le u_m$, then

$$P_i = \frac{E_p A_p}{2h}\left(s_{pi} - s_{p(i+1)}\right) - \frac{\pi r_0 h u \sigma_n}{A + Bu} - \frac{mg}{2},$$
$$s_{p(i+1)} = s_{pi} - \frac{2h}{E_p A_p}\left(P_i + \frac{\pi r_0 h u \sigma_n}{A + Bu} + \frac{mg}{2}\right). \tag{16}$$

If $s_p - s > u_m$, then

$$P_i = \frac{E_p A_p}{2h}\left(s_{pi} - s_{p(i+1)}\right) - \pi r_0 h \tau_m - \frac{mg}{2}, \tag{17}$$

$$s_{p(i+1)} = s_{pi} - \frac{2h}{E_p A_p}\left(P_i + \pi r_0 h \tau_m + \frac{mg}{2}\right). \tag{18}$$

3.2. Numerical Algorithm. Under external forces, the total potential energy II of the pile-soil system equals the deformation energy of the pile and the soil plus the potential energy of the external forces. The numerical method can be introduced for actual calculation: each pile is discretized into n units according to pile length and soil thickness, each of which satisfies the conditions of static balance and continuity; the physical parameters of the target foundation pile are known, while the pile-top load and displacement are unknown. The numerical calculation can be implemented in the following steps (Figure 5):

(1) According to the calculation accuracy and pile length, the pile is divided into n units of the length $h = l/n$, and the mass of each unit is solved.

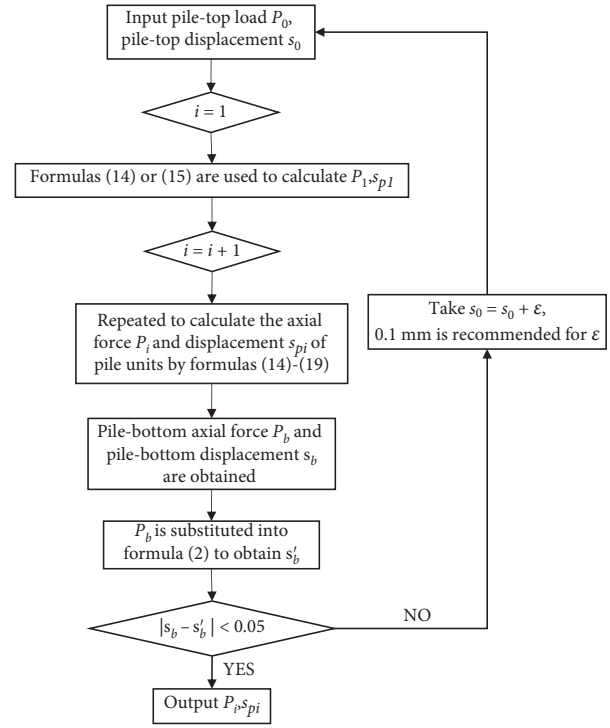

Figure 5: The calculation flow chart.

(2) Let P_0 and s_0 be pile-top load and pile-top displacement, respectively. Then, pile-soil displacement $u = s_i - s_{pi}$ is calculated, while P_1 and s_{p1} are solved by formulas (14) and (15), respectively.

(3) According to pile-soil displacement, Step (2) is repeated to calculate the axial force$P_i$and displacement s_{pi} of pile units by formulas (14)–(18) from top to bottom. If $s_i - s_{pi} = 0$, the axial force P_i of the unit is the maximum axial force of the pile, and the NFR is zero; that is, the node depth is the depth of the neutral point.

(4) Pile-bottom axial force P_b and pile-bottom s_b are obtained through further iterations. Then, P_b is substituted into formula (2) to obtain s_b'. If $|s_b - s_b'|/s_b > 0.05$, then the calculated pile-bottom displacement s_b will be increased by 0.1 mm, and a new iteration will be carried out from Step 1; if $|s_b - s_b'|/s_b < 0.05$, then the calculated pile-bottom displacement s_b is true, and Step 5 will be executed.

(5) The axial force P_i and displacement s_{pi} of each unit are calculated.

4. Comparative Analysis

To verify its engineering applicability, our method was used to calculate the NFR of foundation pile in a construction site, and the calculated results were compared with the data measured from pile-side frictional resistance tests [22]. The iterative calculation program was compiled on MATLAB.

The construction site is formed through land preparation and backfilling over two years. The backfilled soil is 3.8–29.8 m

Table 1: The physical-mechanical parameters of different soil layers.

Soil layer	Compression modulus (MPa)	Poisson's ratio	Cohesion (KPa)	Internal friction angle (°)	Unit weight (kN/m^3)
Fill	9.23	0.35	12.83	14.7	19
Slightly dense pebble	22.15	0.3	0	26	22
Completely weathered mudstone	15.22	0.3	20	25	19

thick. Prior to the construction of the pile foundation, the site was dynamically compacted at the maximum energy level of 18,000 kN·m, with the replacement piers reaching 8–12 m in depth. Some parts of the site were dynamically compacted at the energy level of 3,000 kN·m.

The test piles are cast-in-situ bored piles (diameter: 0.8 m; material: C30 concrete; elastic modulus: 3e7 KPa; weight per unit volume: 24 kN/m^3; Poisson's ratio: 0.16). Among them, 1# and 2# are friction piles, which reach 2 m into the bearing layer of slightly dense pebbles; 3# is the end-bearing pile, which reaches 3 m into the bearing layer of strongly weathered argillaceous siltstone.

During the calculation, the ultimate relative displacement was set to 6 mm. The ultimate frictional resistance was empirically set as per the properties of the soil layers. The physical-mechanical parameters of the surrounding soil are listed in Table 1.

The settlement of the surrounding soil can be calculated by different methods, depending on the actual situation. To pinpoint the transfer law of the pile-side frictional resistance at the site, the measured settlement of the surrounding soil was linearly fitted, and the pile-soil displacement was analyzed to verify the proposed method.

Figure 6 shows the variation of the settlement of the surrounding soil with depths obtained by the linear fitting of the measured settlement. The fitting formula can be expressed as follows:

$$s(z) = 43.789 - 1.353z. \quad (19)$$

The standard error of the intercept of the linear fitting formula was 1.1011, the standard error of the slope was 0.0601, and R^2 was 0.99215. These results basically agree with the measured data. The calculation shows the maximum settlement (43.789 mm) occurs on the surface.

Figure 7 compares the calculated axial force with the measured data. It can be seen that the axial force first increased and then decreased along the pile depth, which is consistent with the distribution law of measured axial force with depth. The maximum axial force appeared at the neutral point.

The calculated axial forces of 1#-3# peaked at 673 kN, 619 kN, and 680 kN, respectively, while their measured axial forces were 655 kN, 586 kN, and 646 kN, respectively. The calculated axial forces were all greater than the measured values. The relative errors of 1#-3# were 2.7%, 5.6%, and 5.0%, respectively.

In addition, the calculated depths of neutral point of 1#-3# were 14.3 m, 14.6 m, and 17.9 m, respectively, while the measured depths of the neutral point were 15 m, 15 m, and

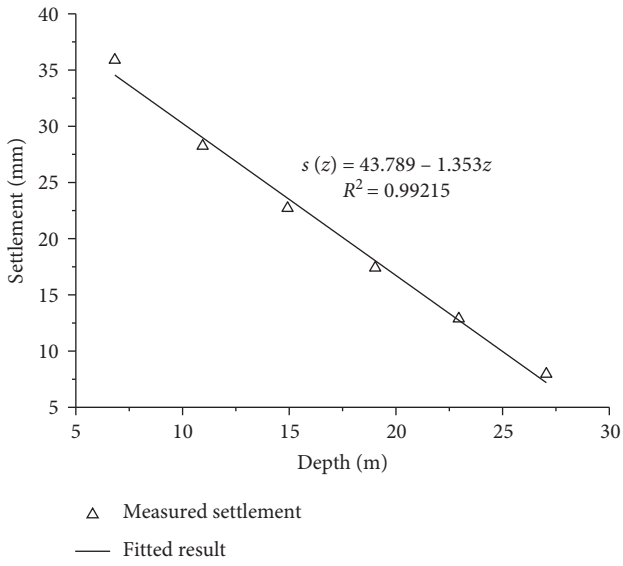

Figure 6: The calculation flow chart.

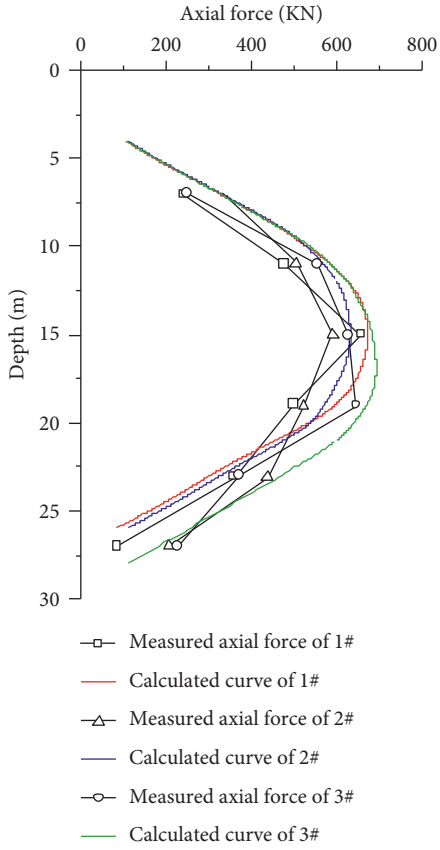

Figure 7: The comparison between calculated axial force and measured axial force.

19 m, respectively. The calculated depths were all shallower than the measured values. The relative errors of 1#-3# were 4.6%, 2.6%, and 5.7%, respectively.

The above data analysis shows that the theoretical distribution of axial force with depth is in line with the test results, while the calculated axial force is slightly larger than the measured value. A possible reason is that the NFR exertion is suppressed effectively within the range of dynamically compacted soil. The calculated value is safer than the measured value.

5. Conclusions

This paper probes deep into the mechanism and transfer law of pile-side frictional resistance in deep fill foundations and then establishes a piecewise calculation model for pile-side frictional resistance. In addition, the theoretical formulas of pile foundation were derived by the energy method. The main conclusions are as follows:

(1) The hyperbolic model was adopted to calculate the pile-side frictional resistance before the pile-soil shear displacement reaches the limit state, and the piecewise calculation model for pile-side frictional resistance was established by combining the hyperbolic model with an effective stress method.

(2) Based on the piecewise calculation model and the reciprocal theorem, the calculation formulas were theoretically derived for the axial force and displacement of the pile in deep fill foundations, in the light of the pile-soil displacement and the potential energy change of the pile-soil system.

(3) Taking a construction site, for example, the distribution of the axial force of the piles along the depth obtained by our theoretical formula basically agrees with that measured in tests. For the three test piles, the maximum error between calculated and measured peak axial forces was 5.6%, and the maximum error between calculated and measured depths of the neutral point was 5.7%. The results indicate that our method has high accuracy and provides a good reference for related engineering practices.

Data Availability

The data used to support the findings of this study are available from the corresponding author upon request.

Conflicts of Interest

The authors declare that they have no conflicts of interest.

Acknowledgments

This work was supported by the National Natural Science Foundation of China (Project no. 51608081) and the Scientific and Technological Research Program of the Chongqing Municipal Education Commission (nos. KJQN201800743 and KJ1600532).

References

[1] X. J. Zhang, H. L. Liu, K. Fei, and Y. F. Gao, "Study on mechanism for negative skin friction of cast-in-situ concrete thin-wall pipe pile," *Rock and Soil Mechanics*, vol. 26, pp. 91–94, 2005.

[2] J. Chen, J. J. Zheng, B. G. Chen, and Y. E. Lu, "Analysis of working behavior of rigid pile composite ground considering influence of negative skin friction," *Rock and Soil Mechanics*, vol. 29, no. 7, pp. 1955–1959, 2008.

[3] H. G. Poulos and N. S. Mattes, "The analysis of down-drag in end-bearing piles," in *Proceedings of the 7th ICSMFE*, pp. 203–209, Sociedad Mexicana de Mecanica de Suelos, Mexico City, September 1969.

[4] H. G. Poulos, "Analysis of the settlement of pile groups," *Géotechnique*, vol. 18, no. 4, pp. 449–471, 1968.

[5] H. G. Poulos and E. H. Davis, "The development of negative friction with time in end-bearing piles," *Australian Geomechanics*, vol. 35, no. 1, pp. 11–20, 1972.

[6] M. H. Zhao, W. He, and W. G. Cao, "Study on calculation of negative skin friction resistance on piles," *Rock and Soil Mechanics*, vol. 25, no. 9, pp. 1442–1446, 2004.

[7] C. B. He, M. H. Zhao, and Y. Lei, "Negative friction computational research of rock-socketed pile based on load transfer method," *Engineering Mechanics*, vol. 31, no. 11, pp. 110–115, 2014.

[8] R. P. Chen, W. H. Zhou, and W. P. Cao, "Improved hyperbolic model of load-transfer for pile-soil interface and its application in study of negative friction of single piles considering time effect," *Chinese Journal of Geotechnical Engineering*, vol. 29, no. 6, pp. 824–830, 2007.

[9] D. Sahoo, B. Mohanty, and A. Maalika Veetil, "Evaluation of bond strength and flash mass on friction surfaced deposition of aluminium 6063 over IS 2062 low carbon steel using different mechtrode face," *Annales de Chimie - Science des Matériaux*, vol. 44, no. 2, pp. 109–119, 2020.

[10] C. Zhao, H. Gong, C. Zhao, and Q. Miu, "Elastoplastic analysis of interface between clay and concrete considering effect of normal stress history," *Chinese Journal of Rock Mechanics and Engineering*, vol. 31, no. 4, pp. 848–855, 2012.

[11] B. H. Fellenius, "Results from long-term measurement in piles of drag load and downdrag," *Canadian Geotechnical Journal*, vol. 43, no. 4, pp. 409–430, 2006.

[12] S. Yamato and M. B. Karkee, "Reliability based load transfer characteristics of bored precast piles equipped with grouted bulb in the pile toe region," *Soils and Foundations*, vol. 44, no. 3, pp. 57–68, 2004.

[13] J. An and C. Sun, "Safety assessment of the impacts of foundation pit construction in metro station on nearby buildings," *International Journal of Safety and Security Engineering*, vol. 10, no. 3, pp. 423–429, 2020.

[14] T. W. Lai, H. Lei, Z. Y. Ji, and Y. Liang, "Effects of cement-modified soil as blocking cushion of saline soil subgrade," *Revue des Composites et des Matériaux Avancés-Journal of Composite and Advanced Materials*, vol. 30, no. 1, pp. 49–53, 2019.

[15] China Academy of Building Sciences, *JGJ94–2008 Technical Code for Building Pile Foundation*, China Architecture and Building Press, Beijing, China, 1994.

[16] B. Zhu, *Computational Soil Mechanics*, Shanghai Scientific and Technical Publishers, Shanghai, China, 1990.

[17] Y. Zheng, J. Mao, and S. Liang, "Negative skin friction of pile foundation considering soil consolidation in high fill site,"

Journal of Jilin University (Engineering and Technology Edition), vol. 47, no. 4, pp. 1075–1081, 2017.

[18] J. Xu, *The Negative Skin Friction Characteristics and Research on Design Method of Rock-Socketed Piles in Deep Recent Filling Soil Areas*, Southwest Jiaotong University, Chengdu, China, 2013.

[19] M. Liu, *"Research on the Calculation and Characteristic of Negative Friction of Pile Foundation in Newly Thick fill*, Hunan University of Science and Technology, Xiangtan, China, 2014.

[20] G. Ye, W. Zheng, and Z. Zhang, "Investigation on distribution of negative friction of frictional piles in large filling sites," *Rock and Soil Mechanics*, vol. 40, no. 1, pp. 440–448, 2019.

[21] M. H. Zhao and S. S. Liu, "Numerical simulation of negative skin friction on single pile in multiple layer deposits," *Chinese Journal of Geotechnical Engineering*, vol. 30, no. 3, p. 336, 2008.

[22] J. K. Lv, *"Study on the Frictional Resistance of Friction Piles after Deep-Filling and Strong ramming*, Southwest University of Science and Technology, Mianyang, China, 2018.